Chemistry Europe
European Chemical Societies Publishing

WILEY VCH

Excellence in Chemistry Research

Announcing our new flagship journal

- Gold Open Access
- Publishing charges waived
- Preprints welcome
- Edited by active scientists

Meet the Editors of *ChemistryEurope*

Luisa De Cola
Università degli Studi di Milano Statale, Italy

Ive Hermans
University of Wisconsin-Madison, USA

Ken Tanaka
Tokyo Institute of Technology, Japan

ChemistrySelect

Research Article
doi.org/10.1002/slct.202200895

Chemistry Europe
European Chemical Societies Publishing

www.chemistryselect.org

Electro, Physical & Theoretical Chemistry

Synthesis of Cinnamoyl-Amino Acid Ester Derivatives and Structure-Activity Relationship Based on Thermal Stability, Dielectric, and Theoretical Analysis

Eray Çalışkan,*[a] Fatih Biryan,[b] Kenan Koran,*[b] Feride Akman,[c] Ahmet Orhan Görgülü,[d] and Ahmet Çetin[a]

In this study, cinnamic acid derivatives were synthesized from the reaction of benzaldehyde derivatives with malonic acid in the presence of pyridine and piperidine. These compounds were then respectively reacted with glycine and L-alanine methyl ester hydrochloride based on triazine methodology to obtain novel cinnamoyl-amino acid ester derivatives. The structure of these compounds were established via ^{1}H, ^{13}C APT, FT-IR, MS and elemental analysis. The synthesized novel compounds were studied in terms of structure-activity relationship based on dielectric, thermal stability, and theoretical analysis. Dielectric analysis was carried out in terms of amino acid type and aromatic substituted group (electron-withdrawing or releasing group factor). Amino acid side chain differences make alanine conjugates have higher ε' values compared to glycine conjugates. Thermal stability analysis was performed for the compounds (10 and 16) with the highest dielectric constants. Thermal decomposition activation energies were calculated as 95 kJ mol^{-1} and 100 kJ mol^{-1} for 10 and 16, respectively. HOMO-LUMO energy levels and other related properties of the target compounds were analyzed and a correlation was observed between HOMO-LUMO energy band gap and dielectric constant.

Introduction

Amino acid conjugates are class of compounds formed by the reaction of amino acid and one or more biologically active molecules such as flavonoids, vitamins, hormones, steroids, fatty acids, and several heterocyclic compounds.[1] Since amide bond formation is key in the synthesis of amino acid conjugates, an effective coupling reagent should be selected in relation to the structure of the organic compounds. The approaches in amide bond formation reactions have some disadvantages due to their low yield, racemization, degradation and difficulties in purification steps. Several types of coupling reagents have been developed to overcome these problems. Thionyl chloride,[2] oxalyl chloride,[3] phosphorous trichloride (PCl_3), and phosphorous pentachloride (PCl_5) are among the most widely used reagents for obtaining acyl chlorides. However, the major disadvantage of the chlorination agents is the formation of HCl during the reaction. Some functional groups such as the Boc group containing amines are sensitive to the acidic environment. 2-chloro-4,6-dimethoxy-1,3,5-triazine CDMT is generally preferred as a coupling reagent since HCl formed in traditional halogenation reactions does not form and a suitable basic environment for acid sensitive groups is provided. Additionally, CDMT is used in the formation of amides, ester, and acid anhydride owing to its high solubility in various organic solvents, its low cost, reactivity and its long-term stability.[4]

Dielectric materials continue to attract attention due to their application areas such as dielectric based capacitors, communication devices, field effect transistors (FETs) and actuators. Dielectric materials are mostly used as electrical insulators since they do not transmit electricity.[5] In the electric field effect, electrons and atoms are displaced, consequently, electrical charge centers shift and electrical polarization occurs. The formed poles provide electrical charge accumulation on the material surface and are therefore used in capacitor production.[6] The electrical properties of the conjugates were evaluated by studying of electron acceptor-donor group effect, conjugation number, amino acid differences in conjugates and effect of the ortho/meta/para positions of aromatic ring in cinnamic acid derivatives.

HOMO, known as the electron donor (filled state), is used to denote the highest occupied molecular orbital, while LUMO, known as the electron acceptor (empty state), is used to denote the lowest unoccupied molecular orbital. The small energy gap between HOMO and LUMO is related to the high polarizability of molecules, low kinetic stability, and high chemical reactivity. In our molecular modeling calculations, the energy of HOMO

[a] Dr. E. Çalışkan, Prof. Dr. A. Çetin
Department of Chemistry, Faculty of Arts and Sciences,
Bingol University, Bingol 12000, Turkey
E-mail: ecaliskan@bingol.edu.tr
[b] Assoc. Prof. Dr. F. Biryan, Assoc. Prof. Dr. K. Koran
Department of Chemistry, Faculty of Science,
Firat University, Elazig 23119, Turkey
E-mail: kkoran@firat.edu.tr
[c] Assoc. Prof. Dr. F. Akman
Vocational School of Food, Agriculture and Livestock,
Bingöl University, Bingol 12000, Turkey
[d] Prof. Dr. A. O. Görgülü
Department of Chemistry, Faculty of Arts and Sciences,
Marmara University, Istanbul 34722, Turkey

Supporting information for this article is available on the WWW under https://doi.org/10.1002/slct.202200895

and LUMO orbitals and the global molecular reactivity descriptors such as electron affinity (EA), ionization potential (IP), electronegativity (χ), global electrophilicity index (ω), chemical potential (μ), chemical hardness (η) and chemical softness (ς) as well as the HOMO-LUMO gap, one of the important measures indicating the electrical breakdown voltage strength, were examined.

Several biological activity studies have been carried out related to such conjugates,[7] but dielectric, the,rmal and theoretical properties in terms of structure-activity relationship of such conjugates have not been studied in detail. Therefore, the main aim of this study was to synthesize new cinnamoyl-amino acid conjugates and evaluate how the different substituents on the structure affect the dielectric constant, thermal stability, and HOMO-LUMO band gap.

Results and Discussion

Chemistry

A series of cinnamic acids were obtained as trans isomers with high yield and purity in the base-catalyzed medium by using Doebner-Knoevenagel condensation over malonic acid. Cinnamic acid derivatives and amino acid methyl esters were synthesized by triazine methodology.[8] The target compounds were obtained by dropwise addition of N-methyl morpholine to the reaction mixture with cinnamic acid, amino acid, and CDMT coupling reagent with high yield in mild conditions (Scheme 1). The structure of these compounds was characterized via ^{1}H, ^{13}C APT, FT-IR, MS, and elemental analysis (Figure S1–39).

The reaction was taken place as one pot synthesis. In the initial step, N-methyl morpholine attacked triazine and then the carboxylic acid derivative (cinnamic acid) reacts to triazine in the presence of N-methyl morpholine, giving the 2-acyloxy-4,6-dimethoxy-1,3,5-triazine compound over the DMTMM intermediate in the second step which is then proceeded to formation of activated ester. The target product is obtained by reacting of free amine (amino acid methyl ester) as nucleophile to activated ester carbonyl. Due to the weak base character of triazine compound, possible by-products and excess of triazine are eliminated using dilute acid and $NaHCO_3$ in the purification process. The proposed mechanism for the synthesis of cinnamic acid conjugates are shown in Scheme 2.

The main proton peaks are clearly seen in Figure 1. ^{1}HNMR analysis for conjugates containing ester moiety reveals that the methyl ester group has been replaced by the carboxylic acid moiety of cinnamic acid. The presence of the $-CH_2$ proton peak (number 11) of the glycine seen in 3.99 ppm together with -NH proton peak at 8.45 ppm indicates that the target structure was formed. The coupling constant of olefinic protons is 15.6 Hz suggesting that the structure is trans positioned. The presence of olefinic =CH peaks and 2 equivalent aromatic =CH protons also indicate the formation of the target structure. The moieties to be considered in the ^{13}CNMR analysis of amino acid conjugates containing the ester group are two carbonyl carbons, one of which belongs to the ester and the other to the amide group. Subsequently, the methyl carbon of the methyl ester and the $-OCH_3$ carbons of the methoxy group may prove the formation of amino acid conjugate. The presence of olefinic carbon peaks and aromatic carbons (-C=C-) from the starting compound can also be presented as additional evidence.

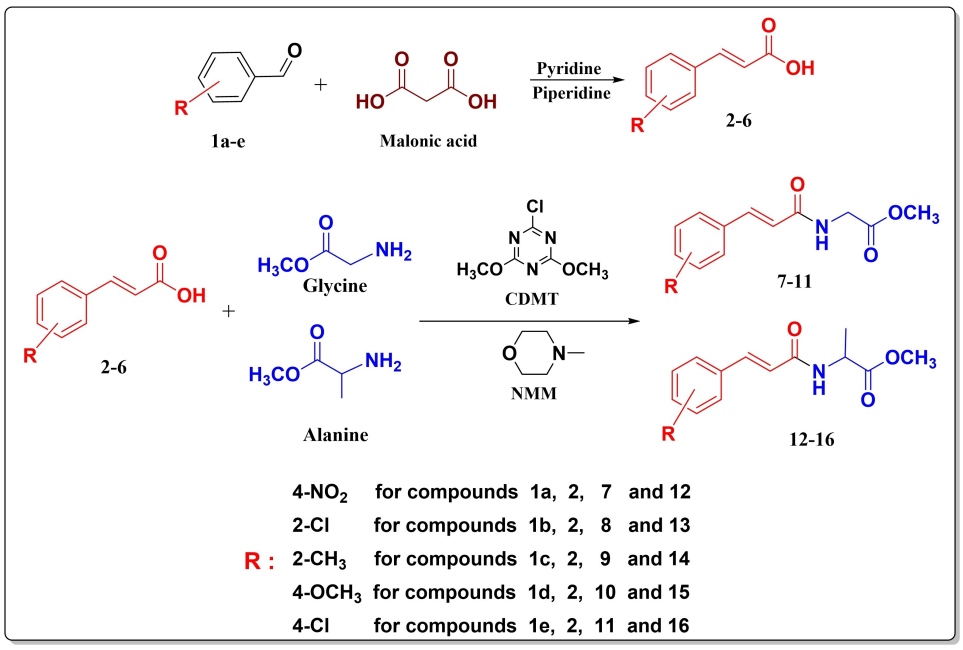

Scheme 1. Synthetic route of cinnamic acids and cinnamoyl amino acid methyl esters.

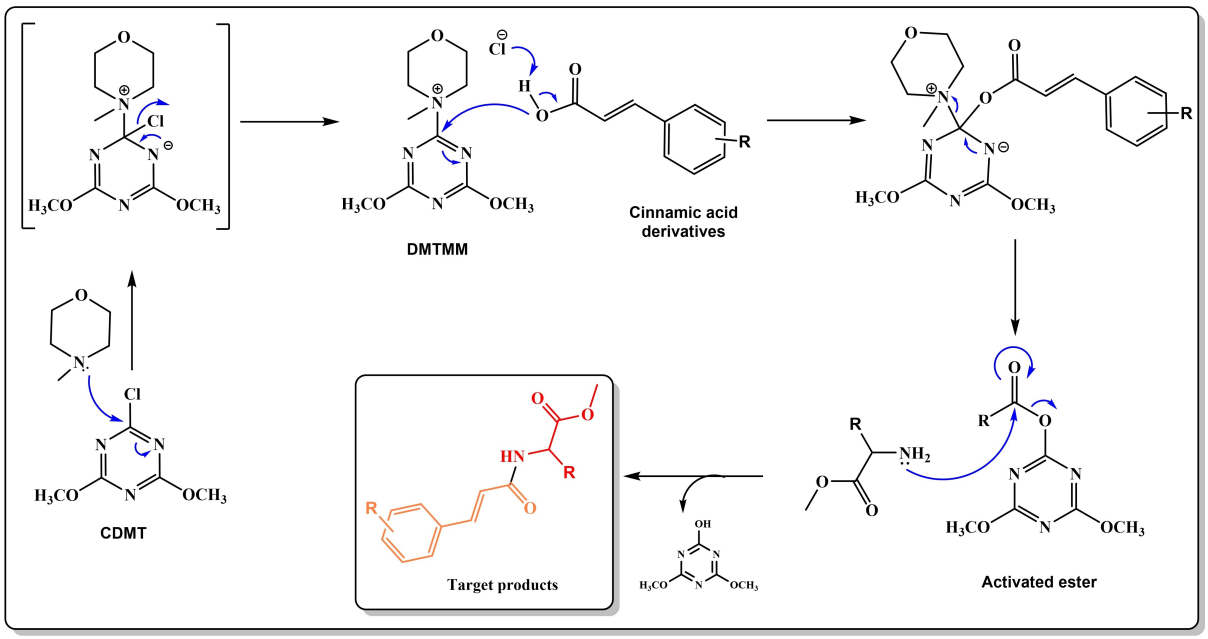

Scheme 2. Proposed mechanism for synthesis of cinnamic acid conjugates.

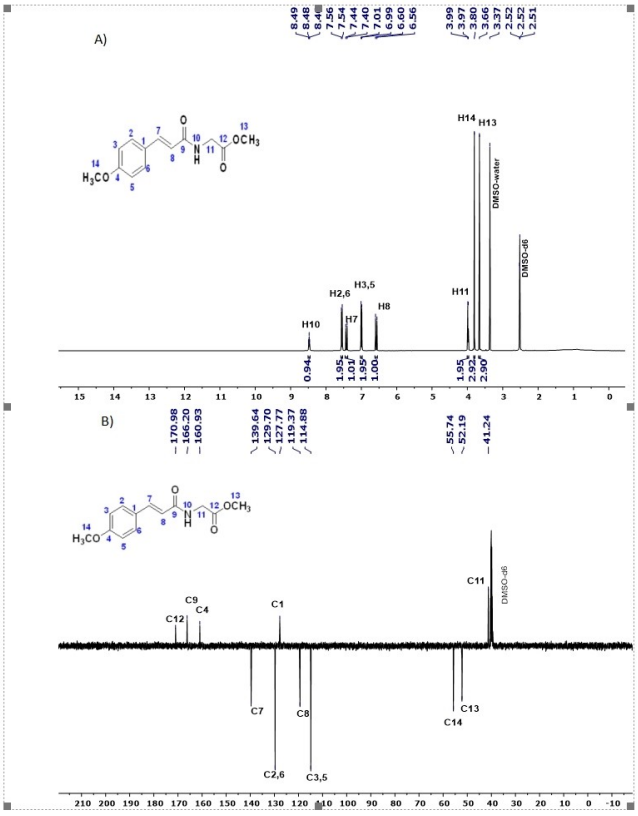

Figure 1. ^{1}H and ^{13}C-APTNMR spectra of compound **10.**

Dielectric measurements

The alternating current (AC) conductivities of the compounds were measured in the range of 1 Hz and 20 kHz. The results were given (Table 1) as conductivity and dielectric over increasing frequency and the conductivity shows changes due to the electrical conductivity which mainly depends on the mobility of electrons or ions. Dielectric analysis based on dielectric constants value were evaluated in terms of amino acid type and aromatic substituted group (electron-withdrawing or releasing group factor) (Figure 2). Initially, amino acid effects on dielectric properties were assessed. Amino acid side chain differences between alanine and glycine (a methyl group), make alanine conjugates have higher ε' values compared to the glycine conjugates. This correlation works inversely for methoxy substituted conjugates. Structure-activity relations analysis revealed that the electron-withdrawing nitro and chloro groups on para position caused the molecules to have the highest ε' value among the others, but this trend is not the same for the electron-donating methoxy group bearing on para position (Table 1).

The dielectric constant indicates how much energy is stored and how much is lost with the electric field applied externally to a compound. Most of the studies related to dielectric properties have been carried out with organic, inorganic, and polymer compounds.[9] As the pure forms of these compounds show low electrical properties, several groups independently aimed to increase the electrical properties of these compounds by using carbon-based, ceramic and various metal composites as fillers as the main method.[10] Huang et al. have managed to increase the dielectric constant to over 400 by forming a composite with a copper atom in phthalocyanine

Table 1. The dielectric constant (ε′), dielectric loss (ε″) and AC conductivity (σ) values in 1 kHz and at 25°C for target conjugates

Entry	ε′	ε″	σ_{ac} (Siemens cm^{-1})	log σ_{ac}
7	7,481	0,289	4.16×10^{-9}	−8,380
8	6,774	0,261	3.76×10^{-9}	−8,424
9	7,142	0,304	3.97×10^{-9}	−8,401
10	7,938	0,317	4.41×10^{-9}	−8,354
11	7,584	0,307	$4.22\ x10^{-9}$	−8,375
12	8,250	0,341	4.59×10^{-9}	−8,338
13	6,873	0,289	3.82×10^{-9}	−8,417
14	8.093	0.078	$5.22x\ 10^{-9}$	−8.282
15	7,871	0,328	$4,38\times10^{-9}$	−8,358
16	8,338	0,339	4.64×10^{-9}	−8,333

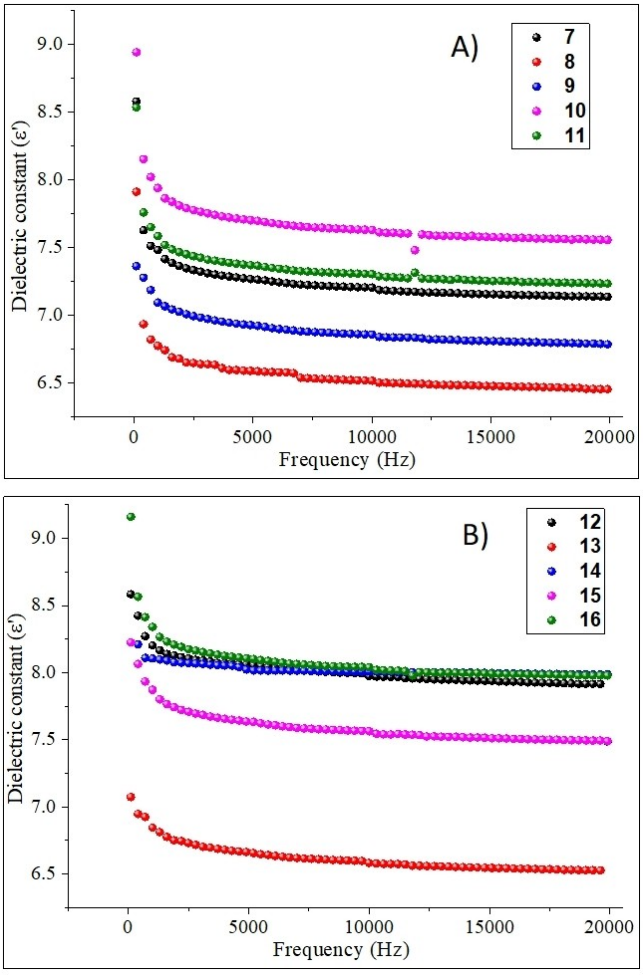

Figure 2. Comparison of glycine (upper panel) and alanine (bottom panel) conjugates based on dielectric constant (ε′).

compounds.[11] In another study, the dielectric constant of the compounds obtained by integrating organic photovoltaic (OPV) into semiconductors with high dielectrics was measured to around 16.[12]

Studies on the dielectric properties of the compounds containing conjugated p electrons in its structure have increased in recent years. The dielectric properties of chalcone derivatives which are structurally similar to cinnamic acid compounds have been studied by several groups in recent years.[13] In the light of these studies, the effects of increasing frequency and temperature on dielectric properties of chalcone derivatives were examined. The obtained results showed that they can be used in various optical and electrical applications such as light-emitting diode, solar cell and nano-sized electronic devices due to their conductive and semiconductor properties.[14]

Thermal Behavior Analysis

Thermal stability analysis was performed for the compounds (**10** and **16**) with highest dielectric constants. TGA curves at different heating rates for **10** and **16** are given in Figure 3. From the TGA curves of the compounds at 10 °C/min heating rate, the initial mass loss temperature was determined as 186 °C for compound **16** and 226 °C for compound **10** suggesting that degradation happens in a single-stage for both compounds. In addition, the maximum decomposition temperatures (T_{max}) determined from the derivative curves (DTG) in Figure 3 are 272 °C and 305 °C, respectively revealing that the thermal stability of compound **10** is higher. Thermal analysis results are summarized in Table 2.

Flynn-Wall-Ozawa (FWO) integral method, which is independent of reaction order, was used to calculate the thermal decomposition activation energy value for both compounds. This method is one of the most common methods used to determine the activation energy based on experimental results without needing to know the reaction sequence and degradation mechanism and provides reliable and accurate evaluations for calculating Ea from TGA curves.[15] According to the recommendation of the kinetic committee of the International Confederation of Thermal Analysis and Calorimetry (ICTAC),[15c] the Flynn-Wall-Ozawa (FWO) analysis suggests a noteworthy advancement in the accuracy of reasonable evaluation of activation energy by TGA. The FWO method provides data about the dependence of activation energy during transformation.

For this purpose, log β values against 1/T are plotted. The slopes of the obtained lines were determined and their activation energies were calculated according to the equation (1).[16]

$$\ln(\beta) = \text{constant} - 1.052\ \frac{E_a}{R.T} \qquad (1)$$

TGA and DTG curves of **10** and **16** at different heating rates are shown in Figure 3. Thermal decomposition activation energies corresponding to each conversion value were calculated separately. In this case, average activation energy values for compound **16** and compound **10** in the 2% - 80% decay range were calculated as 95.25 kJ mol^{-1} and 100.16 kJ mol^{-1}, respectively. The average activation energy value for diphenyl alanine compound was calculated as 148 kJ mol^{-1} according to FWO method.[17] The change of activation energy values against conversion percentages is shown (Figure 4). The activation

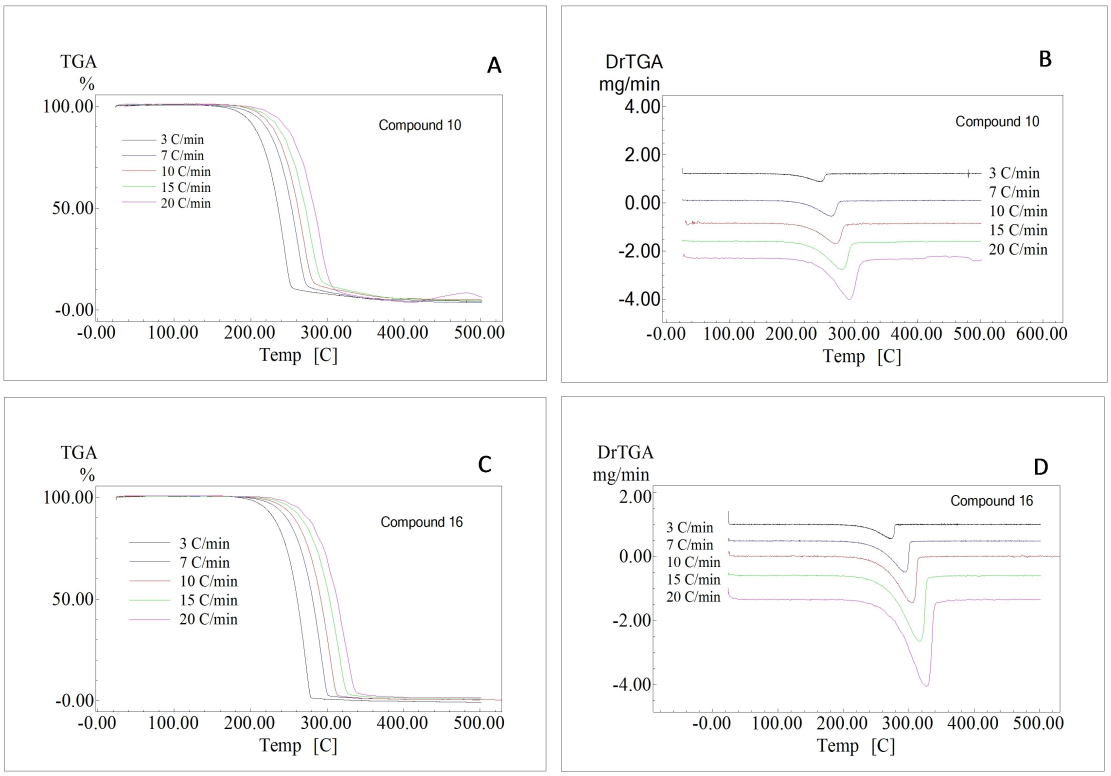

Figure 3. TGA (left panels) and DTG (right panels) curves of **10** and **16** at different heating rates.

Table 2. TGA results of compounds **10** and **16**.

Heating rate	$T_{initial}$ (°C)		$T_{\%50}$ (°C)		T_{final} (°C)		T_{max} (°C)	
(°C min^{-1})	10	16	10	16	10	16	10	16
3	204	171	261	235	283	260	272	247
7	210	175	280	252	304	272	295	261
10	226	186	292	261	319	284	305	272
15	237	189	305	271	331	296	316	282
25	246	207	317	283	342	307	327	291

energy was calculated as the minimum at the initial values at which the decomposition started. It is estimated that this is due to the evaporation of small molecules and the breaking of weak bonds during TGA analysis. The activation energy calculated using thermograms at different heating rates is based on the mass loss, not the products formed during decomposition. At higher heating rates, a heat inconsistency occurs between the outer surface of the deteriorated material and its interior. Therefore, with the increase of the heating rate, the decomposition temperatures of the materials also increase, and due to the increase in the heating rate, decomposition reactions occur on the outer surface at higher temperatures.[13d,18]

HOMO and LUMO Analysis

The 3D plots of HOMO and LUMO for the **7**–**11** and **12**–**16** molecules were calculated using the Gaussian 09 W package[19] and GaussView 5.0,[20] and indicated in Figure 5. The green and red colors in Figure 5 indicate the positive and negative phases in the molecule, respectively, and represent charge transfer within the molecule. Energy of HOMO and LUMO orbitals and the global molecular reactivity descriptors such as electron affinity (EA), ionization potential (IP), electronegativity (χ), global electrophilicity index (ω), chemical potential (μ), chemical hardness (η) and chemical softness (ς) were calculated using the B3LYP/6-31+G(d,p) technique and given in Table 3.

The parameters are defined as:[21]

$$\text{Ionization potential; } \boldsymbol{IP} = -\boldsymbol{E_{HOMO}} \quad (2)$$

$$\text{Electron affinity; } \boldsymbol{EA} = -\boldsymbol{E_{LUMO}} \quad (3)$$

$$\text{Electronegativity; } \chi = -{}^{1}\!/_{2}(\boldsymbol{E_{LUMO}} + \boldsymbol{E_{HOMO}}) \quad (4)$$

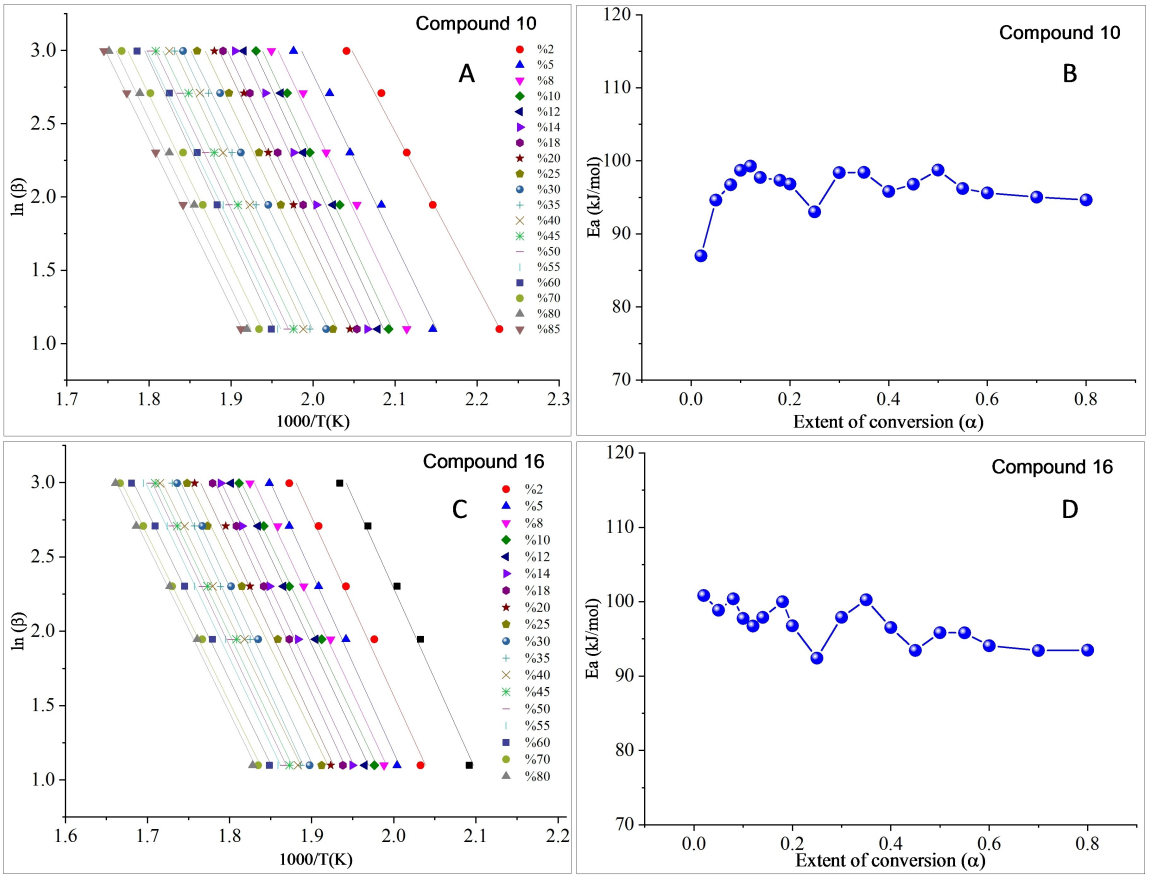

Figure 4. Flynn-Wall-Ozawa curves (left panels) and the dependence of E_a on the extent of conversion at different conversion (right panels) for **10** and **16.**

Table 3. Some electronic structure parameters for the **7–11** and **12–16** molecules calculated at B3LYP/6-31G + (d,p) basis set.

Parameters	Values (eV)									
	7	8	9	10	11	12	13	14	15	16
E_{HOMO}[a]	−7.2127	−6.6750	−6.4355	−5.9868	−6.5555	−7.1925	−6.6592	−6.4222	−5.6635	−6.5416
E_{LUMO}[b]	−3.2044	−2.0169	−1.7908	−1.6485	−2.0877	−3.1930	−2.0063	−1.7837	−1.1709	−2.0779
Eg[c]	4.0082	4.6580	4.6447	4.3383	4.4678	3.9995	4.6529	4.6385	4.4926	4.4638
IA[d]	7.2127	6.6750	6.4355	5.9868	6.5555	7.1925	6.6592	6.4222	5.6635	6.5416
EA[e]	3.2044	2.0169	1.7908	1.6485	2.0877	3.1930	2.0063	1.7837	1.1709	2.0779
χ[f]	5.2085	4.3459	4.1131	3.8176	4.3216	5.1928	4.3327	4.1029	3.4172	4.3097
μ[g]	−5.2085	−4.3459	−4.1131	−3.8176	−4.3216	−5.1928	−4.3327	−4.1029	−3.4172	−4.3097
η[h]	2.0041	2.3290	2.3224	2.1692	2.2339	1.9998	2.3264	2.3192	2.2463	2.2319
ζ[i]	0.4990	0.4294	0.4306	0.4610	0.4476	0.5001	0.4298	0.4312	0.4452	0.4481
ω[j]	6.7683	4.0547	3.6424	3.3594	4.1801	6.7420	4.0346	3.6292	2.5992	4.1610

[a]; energy of HOMO, [b]; energy of LUMO, [c]; energy gap between LUMO and HOMO, [d]; ionization potential, [e]; electron affinity, [f]; electronegativity, [g]; chemical potential, [h]; chemical hardness, [I]; chemical softness, [j];global electrophilicity index.

Global electrophilicity index; $\omega = \frac{\mu^2}{2\eta}$ (5)

Chemical potential; $\mu = {}^1/_2(E_{LUMO} + E_{HOMO})$ (6)

Chemical hardness; $\eta = {}^1/_2(E_{LUMO} - E_{HOMO})$ (7)

Chemical softness; $\varsigma = \frac{1}{\eta}$ (8)

Molecular Electrostatic Potential (MEP) Analysis

MEP surface maps of **7–11** and **12–16** molecules were determined using B3LYP/6-31 +G(d,p) software and the electron distribution of the molecules was studied.[22] The MEP

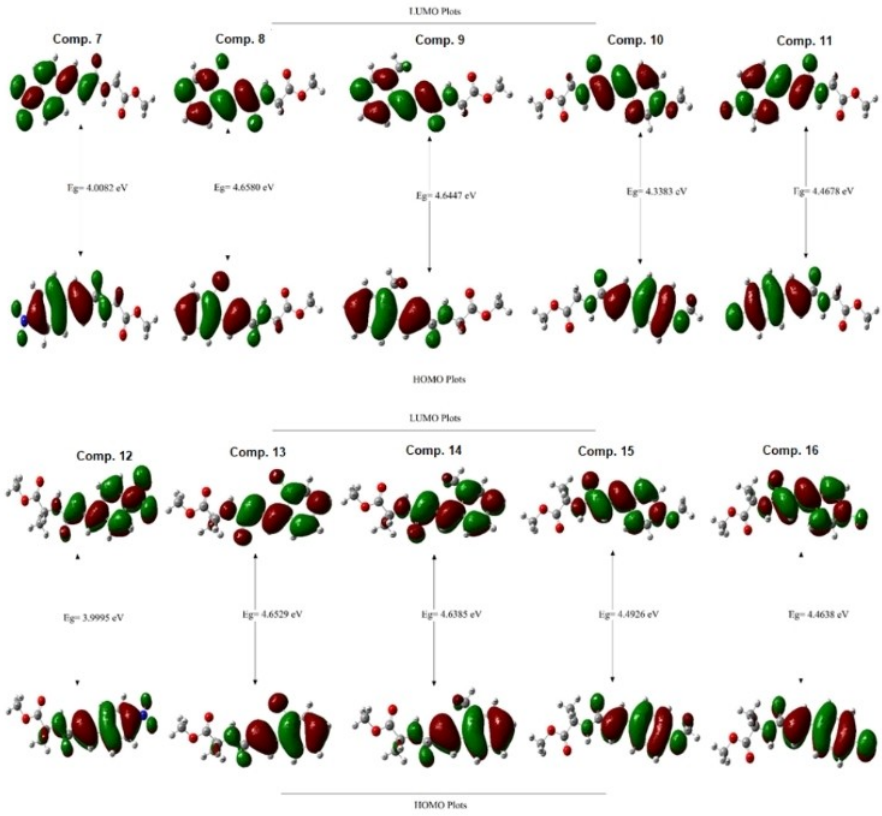

Figure 5. HOMO-LUMO energy levels of target compound **7**–**16.**

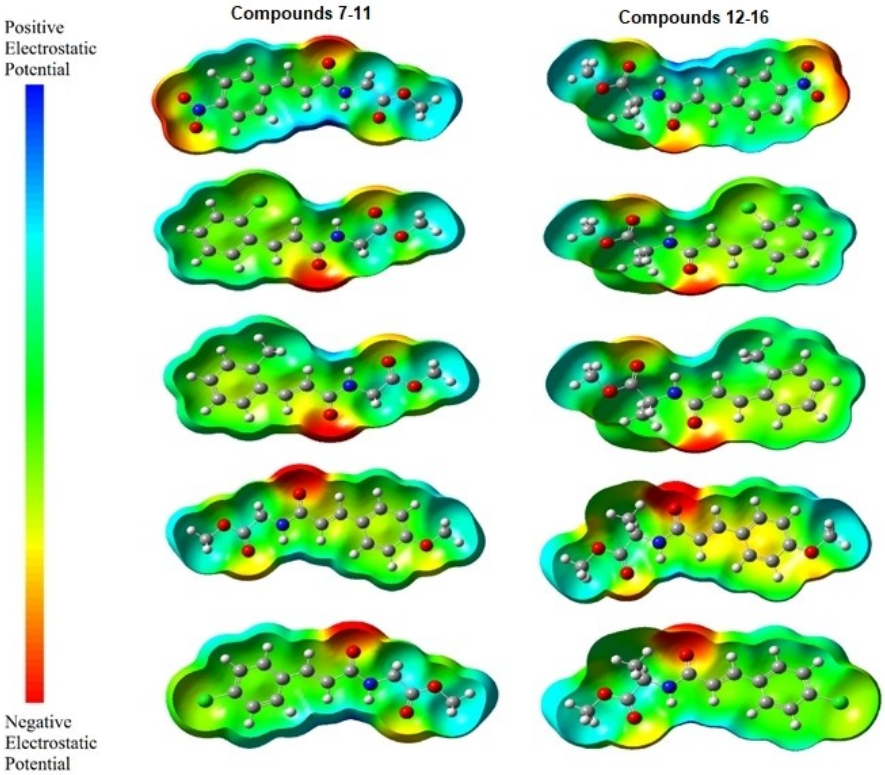

Figure 6. Molecular electrostatic potential surfaces of **7**–**11** and **8**–**16** molecules in B3LYP/6-31 + G (d,p).

map is used to describe the electron density of molecules as well as hydrogen bond interactions, electrophilic and nucleophilic attack regions in three dimensions.[23] The positive electrostatic potential (blue coded region) in a molecule refers to the repulsion of a proton by atomic nuclei in regions with low electron density, while the negative electrostatic potential (red coded region) refers to the attraction of a proton by condensing the electron density. Decrease in potential is represented by color in the order of blue > green > yellow > orange > red. The MEP surfaces of **7**–**11** and **12**–**16** in the range from −0.0500 a.u. (red) to 0.0500 a.u. (blue) were represented in Figure 6. The negative potential region related to electrophilic attack region is on carbonyl and nitro groups due to electronegative oxygen atoms,[24] while the positive potential region related to nucleophilic attack region is on hydrogen atoms. The MEP analysis demonstrates that the oxygen atoms in the carbonyl and nitro groups of **7**–**11** and **12**–**16** molecules in the maximum negative region are the most reactive part of electrophilic attack region.

The small energy gap between HOMO and LUMO is associated with a molecule's high polarizability, low kinetic stability, and high chemical reactivity. For the **7**–**11**, the values of the HOMO-LUMO energy gap were calculated as 4.00, 4.65, 4.64, 4.33, and 4.46 eV, respectively, while the values of the HOMO-LUMO energy gap for **12**–**16**, are 3.99, 4.65, 4.63, 4.49 and 4.46 eV, respectively, demonstrating that charge transfer occurs within 7 and 12 more than others (Table 1). The energy gap among **12**–**16** (**possess methyl moiety**), which is different from **7**–**11** (**no methyl moiety present in the structure**) slightly decreased compared to **7**–**11**, except for the compounds **10** and **15**. The compounds with smaller energy gaps (**12**, **13**, **14**, and **16**) show lower kinetic stability, and higher chemical reactivity than **7**, **8**, **9**, and **11**. The lower the energy gap a compound has, the higher its polarizability is due. The fact that a compound has high polarizability causes an increase in the dielectric constant. In this context, it is seen that there is a correlation in the comparisons between the energy gap values of the compounds and their dielectric constants. Except for the compounds with methoxy substituents (**10**–**15**), a correlation appeared between the other compounds.

Conclusion

In summary, new cinnamic acid-amino acid hybrid compounds were synthesized under mild and effective conditions via triazine methodology. Thermal, dielectric, and theoretical analysis were performed. Structure-activity relationship based on the electron-releasing and electron-withdrawing groups effect was conducted in terms of dielectric constant and HOMO-LUMO band gap. The compounds that have the highest dielectric constant were selected to perform thermal stability analysis to calculate the activation energies and thermal decomposition properties. The results exhibit both conjugates (**10**–**16**) have similar thermal behavior trends. Theoretical analysis (DFT) studies were conducted to reveal the relationship of structure and HOMO-LUMO energy levels. The results indicate that there is a correlation among conjugates except strong electron-withdrawing nitro containing conjugates, the conjugates **10** and **16** have the highest dielectric constant value similarly have the smallest HOMO-LUMO band gap.

Supporting Information Summary

Experimental Section, FT-IR, ^{1}H-, $^{13}C_{APT}$-NMR spectra of all synthesized compounds were given in the Supporting Information section.

Acknowledgements

In this study, all data of synthesized compounds and dielectric measurements were produced from Eray Çalışkan's Ph.D. thesis, which was granted by Bingöl University Scientific Research Council (Project no: BAP-FEF.2018.000.003) and supported by Bingöl University for the server and Bitlis Eren University for Gaussian software.

Conflict of Interest

The authors declare no conflict of interest.

Data Availability Statement

The data that support the findings of this study are available in the supplementary material of this article.

Keywords: Amino acid · Cinnamic acid · Dielectric · Structure-activity · Thermal stability

[1] a) S. S. Panda, M. A. Ibrahim, H. Küçükbay, M. J. Meyers, F. M. Sverdrup, S. A. El-Feky, A. R. Katritzky, *Chem. Biol. Drug Des.* **2013**, *82*, 361–366; b) S. Sahu, S. S. Panda, A. M. Asiri, A. R. Katritzky, *Synthesis* **2013**, *45*, 3369–3374.
[2] W. Chu, Z. Tu, E. McElveen, J. Xu, M. Taylor, R. R. Luedtke, R. H. Mach, *Bioorg. Med. Chem.* **2005**, *13*, 77–87.
[3] R. Adams, L. H. Ulich, *J. Am. Chem. Soc.* **1920**, *42*, 599–611.
[4] a) K. Venkataraman, D. R. Wagle, *Tetrahedron Lett.* **1979**, *20*, 3037–3040; b) M. Kunishima, C. Kawachi, F. Iwasaki, K. Terao, S. Tani, *Tetrahedron Lett.* **1999**, *40*, 5327–5330; c) Z. J. Kamiński, P. Paneth, J. Rudziński, *J. Org. Chem.* **1998**, *63*, 4248–4255.
[5] I. Betova, M. Bojinov, E. Lankinen, G. Sundholm, *J. Electroanal. Chem. Interfacial Electrochem.* **1999**, *472*, 20–32.
[6] M. Campos, P. A. P. Nascente, *Synth. Met.* **2010**, *160*, 1513–1519.
[7] a) X.-k. Long, L.-Q. Liao, Y.-F. Zeng, Y. Zhang, F. Xiao, C. Li, Y. Guo, *ChemistrySelect* **2019**, *4*, 5662–5666; b) M. Daniluk, W. Buchowicz, M. Koszytkowska-Stawińska, K. Jarząbek, K. N. Jarzembska, R. Kamiński, M. Piszcz, A. E. Laudy, S. Tyski, *ChemistrySelect* **2019**, *4*, 11130–11135; c) A. Soltani Hekmat, M. Farjam, K. Javanmardi, S. Behrouz, E. Zarenezhad, M. N. Soltani Rad, *ChemistrySelect* **2021**, *6*, 13595–13600.
[8] a) C. E. Garrett, X. Jiang, K. Prasad, O. Repič, *Tetrahedron Lett.* **2002**, *43*, 4161–4165; b) E. Çalışkan, K. Koran, A. O. Görgülü, A. Çetin, *J. Mol. Struct.* **2020**, *1222*, 128830.
[9] a) F. Biryan, G. Pihtili, *J. Polym. Res.* **2021**, *28*, 382; b) F. Biryan, G. Pihtili, K. Demirelli, *J. Therm. Anal. Calorim.* **2020**, *139*, 3871–3885; c) F. Yakuphanoglu, M. Okutan, Q. Zhuang, Z. Han, *Phys. B* **2005**, *365*, 13–19; d) M. R. Vengatesan, S. Devaraju, A. A. Kumar, M. Alagar, *High Perform. Polym.* **2011**, *23*, 441–456.
[10] a) M. T. Sebastian, R. Ubic, H. Jantunen, *Int. Mater. Rev.* **2015**, *60*, 392–412; b) P. Nanni, M. Viviani, V. Buscaglia, in *Handbook of Low and High Dielectric Constant Materials and Their Applications* (Ed.: H. Singh Nalwa), Academic Press, Burlington, **1999**, 429–455.

[11] V. Bobnar, A. Levstik, C. Huang, Q. M. Zhang, *Phys. Rev. B.* **2005**, *71*, 041202.
[12] J. Brebels, J. V. Manca, L. Lutsen, D. Vanderzande, W. Maes, *J. Mater. Chem. A* **2017**, *5*, 24037–24050.
[13] a) M. Okutan, Y. Yerli, S. E. San, F. Yılmaz, O. Günaydın, M. Durak, *Synth. Met.* **2007**, *157*, 368–373; b) K. Koran, F. Özen, F. Biryan, A. O. Görgülü, *J. Mol. Struct.* **2016**, *1105*, 135–141; c) K. Koran, *J. Mol. Struct.* **2019**, *1179*, 224–232; d) F. Biryan, K. Demirelli, *Adv. Polym. Technol.* **2018**, *37*, 1994–2012.
[14] a) A. Sharma, K. M. Batoo, O. M. Aldossary, S. Jindal, N. Aggarwal, G. Kumar, *J. Mater. Sci. Mater. Electron.* **2021**, *32*, 313–322; b) T. A. Taha, *Polym. Bull.* **2019**, *76*, 903–918; c) M. Shkir, S. AlFaify, *J. Mater. Res.* **2019**, *34*, 2765–2774; d) I. Rivera, A. Kumar, F. Mendoza, R. S. Katiyar, *Phys. B* **2008**, *403*, 2423–2430.
[15] a) W. Du, G. Wang, Y. Wang, X. Liu, *Appl. Therm. Eng.* **2019**; b) L. Núñez, F. Fraga, M. R. Núñez, M. Villanueva, *Polymer* **2000**, *41*, 4635–4641; c) S. Vyazovkin, K. Chrissafis, M. L. Di Lorenzo, N. Koga, M. Pijolat, B. Roduit, N. Sbirrazzuoli, J. J. Suñol, *Thermochim. Acta* **2014**, *590*, 1–23.
[16] F. Biryan, K. Demirelli, *J. Mol. Struct.* **2019**, *1186*, 187–203.
[17] M. A. Ziganshin, A. V. Gerasimov, S. A. Ziganshina, N. S. Gubina, G. R. Abdullina, A. E. Klimovitskii, V. V. Gorbatchuk, A. A. Bukharaev, *J. Therm. Anal. Calorim.* **2016**, *125*, 905–912.
[18] G. K. Gupta, M. K. Mondal, *J. Therm. Anal. Calorim.* **2019**, *137*, 1431–1441.
[19] H. B. S. G. W. T. M. J. Frisch, G. E. Scuseria, M. A. Robb, J. R. Cheeseman, G. Scalmani, V. Barone, B. Mennucci, G. A. Petersson, H. Nakatsuji, M. Caricato, X. Li, H. P. Hratchian, A. F. Izmaylov, J. Bloino, G. Zheng, J. L. Sonnenberg, M. Hada, M. Ehara, K. Toyota, R. Fukuda, J. Hasegawa, M. Ishida, T. Nakajima, Y. Honda, O. Kitao, H. Nakai, T. Vreven, J. A. Montgomery, Jr., J. E. Peralta, F. Ogliaro, M. Bearpark, J. J. Heyd, E. Brothers, K. N. Kudin, V. N. Staroverov, T. Keith, R. Kobayashi, J. Normand, K. Raghavachari, A. Rendell, J. C. Burant, S. S. Iyengar, J. Tomasi, M. Cossi, N. Rega, J. M. Millam, M. Klene, J. E. Knox, J. B. Cross, V. Bakken, C. Adamo, J. Jaramillo, R. Gomperts, R. E. Stratmann, O. Yazyev, A. J. Austin, R. Cammi, C. Pomelli, J. W. Ochterski, R. L. Martin, K. Morokuma, V. G. Zakrzewski, G. A. Voth, P. Salvador, J. J. Dannenberg, S. Dapprich, A. D. Daniels, O. Farkas, J. B. Foresman, J. V. Ortiz, J. Cioslowski, D. J. Fox„, Revision C.01 ed., Gaussian, Inc.„, Wallingford CT, **2010**.
[20] R. Dennington, Keith, T. Millam, J., Version 5. ed., Shawnee Mission, Semichem Inc., **2010**.
[21] a) T. Koopmans, *Physica* **1934**, *1*, 104–113; b) R. S. Mulliken, *J. Chem. Phys.* **1934**, *2*, 782–793; c) R. G. Pearson, *J. Am. Chem. Soc.* **1985**, *107*, 6801–6806; d) W. Yang, R. G. Parr, *Proc. Nat. Acad. Sci.* **1985**, *82*, 6723–6726; e) R. G. Parr, R. G. Pearson, *J. Am. Chem. Soc.* **1983**, *105*, 7512–7516; f) R. G. Parr, L. v. Szentpály, S. Liu, *J. Am. Chem. Soc.* **1999**, *121*, 1922–1924.
[22] K. S. Jane, S. Murray, *Molecular Electrostatic Potentials Concepts and Applications*, 1st Edition ed., Elsevier, **1996**.
[23] a) E. Scrocco, J. Tomasi, in *Advances in Quantum Chemistry, Vol. 11* (Ed.: P.-O. Löwdin), Academic Press, **1978**, 115–193; b) F. J. Luque, J. M. López, M. Orozco, *Theor. Chem. Acc.* **2000**, *103*, 343–345.
[24] a) H. G. O. Becker, *J. Prakt. Chem.* **1978**, *320*, 879–880; b) Yeung, S. Hong, E. J. Corey, *J. Am. Chem. Soc.* **2006**, *128*, 6310–6311.

Submitted: March 24, 2022
Accepted: May 9, 2022